Ignition Characteristics of Turbulent Combustible Mixtures by Composite Sparks

O.Aoki, K.Ishii*, H.Nomura**, Y.Ujiie** and M.Kono

Department of Aerospace Engineering
University of Tokyo
7-3-1 Hongo, Bunkyo-ku, Tokyo 113
Japan
* *Yokohama National University*
** *Nihon University*

ABSTRACT

In order to clarify the characteristic of ignition of combustible mixtures by composite sparks under high turbulence intensity conditions, minimum ignition energy was measured by using the experimental apparatus which had been developed to produce high intensity turbulence with minimum mean flow by mutual collision of mixture jets at the center of a combustion chamber and by using the ignition system which could vary energies of a capacitance component and an inductance component independently. The experimental results show that ignition ability is much improved by the addition of an inductance component to a capacitance component. This improvement is pronounced in case of turbulent mixtures of high intensity. In addition, a numerical simulation was performed to study the mechanism of flame kernel development. A set of partial differential equations in two-dimensional cylindrical coordinates was resolved by Large Eddy Simulation in the numerical simulation. Minimum ignition energy and turbulence intensity in the spark gap were estimated from the numerical simulation. The calculated results suggest that inductance component has the effect to keep a flame kernel near the spark gap and the effect of turbulence suppression in the spark gap.

INTRODUCTION

In spark ignition engines, lean mixtures with high intensity turbulence have been adopted to reduce fuel consumption and to improve exhaust emissions. In such conditions, a spark igniter of higher ignition ability is required. The conventional spark igniter produces composite sparks which consists of a capacitance component leading to a short duration spark and an inductance component leading to a weak and long duration spark. In the present work, a specially designed experimental apparatus was developed to realize high intensity turbulence with minimum mean flow. An ignition system which could generate simulated composite sparks was also developed. Minimum ignition energy on the energy distribution of composite sparks was measured in various turbulence intensity to investigate the effect of composite sparks on ignitions under high turbulence intensity conditions. In addition, a numerical simulation calculating distributions of temperature and velocity was made to study the mechanism of flame kernel development. Minimum ignition energy and turbulence intensity in the spark gap were estimated from the numerical simulation.

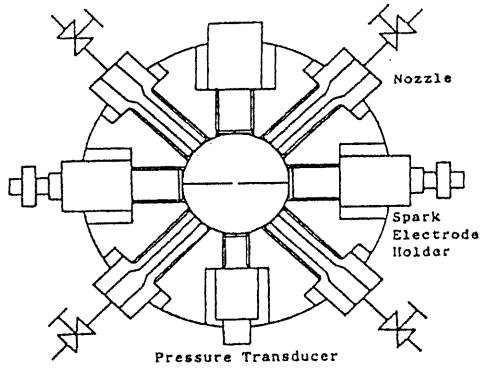

Fig. 1 Combustion chamber

EXPERIMENTAL APPARATUS

A sectional view of the combustion chamber is shown in Fig. 1. The combustion chamber is cylindrical, with internal diameter of 40 mm and height of 30 mm. Two glass windows are attached on both faces. A set of spark electrode holders is attached on the side wall of the combustion chamber. Spark electrodes are stainless wires of 0.2 mm in diameter, whose tips are sharpened to keep spark path at the center of the axes of the spark electrodes. The spark gap width is kept 1.0 mm. Four nozzles of 3 mm in diameter are attached on the side wall of the combustion chamber. A mixture flows into the combustion chamber through these nozzles. High intensity turbulence is generated at the center of the combustion chamber by mutual collision of jets of mixture through these nozzles. The velocity of the individual jet was adjusted by the valve at each nozzle inlet so that the creation of mean flow at the

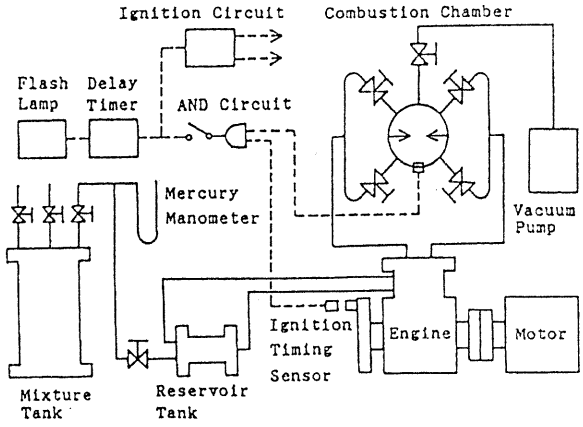

Fig. 2 Experimental apparatus

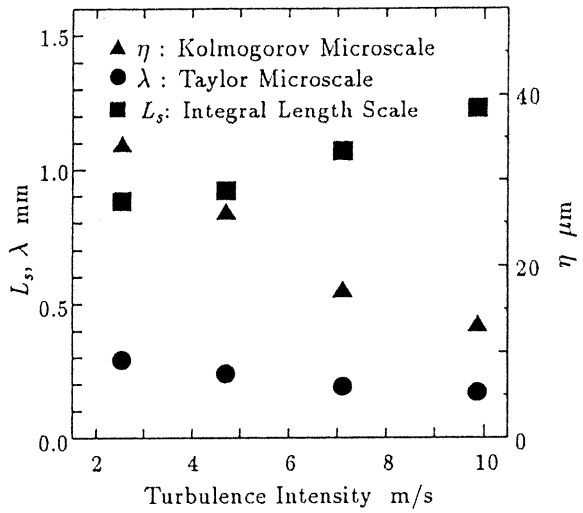

Fig. 4 Turbulent scales

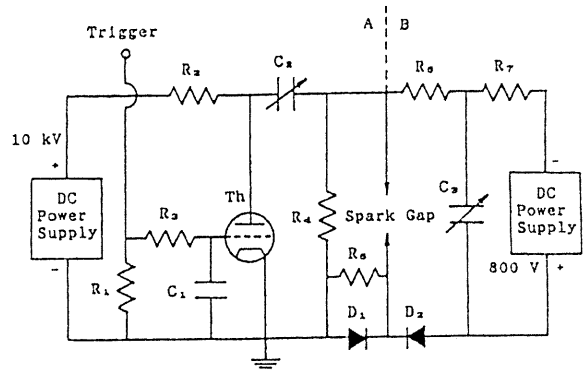

Fig. 3 Ignition system

center of the combustion chamber might be minimized.

A schematic diagram of the experimental apparatus is shown in Fig. 2. A four-stroke single cylinder engine driven by an electric motor was used as a pump to feed mixture into the combustion chamber. The engine has a displacement of 258 cm^3, and a compression ratio of 6.5. The intake and exhaust manifolds are connected to the reservoir tank. Two manifolds connected to the combustion chamber are fastened to the cylinder head of the engine. In operation, a propane-air mixture containing 4.7% by volume of propane was drawn from a mixture tank and supplied to the combustion chamber, the engine, and the reservoir tank at atmospheric pressure and room temperature. Then, the engine was driven by the electric motor. In the compression stroke, the mixture was pumped through the cylinder head manifolds to the combustion chamber. In the expansion stroke, the mixture was sucked from the combustion chamber and returned to the engine. The turbulence intensity in the combustion chamber was varied by changing the engine speed.

The ignition system was designed to generate composite sparks which comprised of a capacitance spark and an inductance spark. A block diagram of the electric circuit is shown in Fig. 3. The high voltage supply charged the condenser C_2, through the charging resistance R_2, to 10 kV. Then, the thyratron was switched on by a trigger pulse, and the capacitance component was generated. This acted as a trigger for the inductance component from the condenser C_3, which was charged to 800 V. Although the post capacitance spark is not an inductance component because of being generated by discharge of a condenser, this is called an inductance component in the present work. The spark energy was controlled by changing the electrostatic capacity of the condenser. The voltage and current of the spark discharge were measured by a voltage probe (TEKTRONIX P6015) and a current probe (TEKTRONIX P6021), respectively. The spark energy was determined by integration of the voltage multiplied by the current during the spark discharge. The ignition timing was set at 35° BTDC in the compression stroke of the engine, when the velocity of the mixture jet is maximum. The triggering system prevented any ignition pulse in the exhaust stroke. At each experimental condition, the ignition experiment was conducted 30 times to determine the ignition probability. The minimum ignition energy was defined as the ignition energy yielding a 50% ignition probability.

The velocity fluctuation at the center of the combustion chamber was measured to estimate turbulence intensity. The velocity component normal to the axis of the combustion chamber was measured with a laser doppler velocimeter (DANTEC 55X). Scattered light was detected by a photomultiplier (KANOMAX MODEL 1961). A burst spectrum analyzer (DANTEC 57N10) was used as a signal processor. The velocity component parallel to the axis of the combustion chamber was measured by a hot wire anemometer (SOKKEN HC-30) having a tungsten wire probe of 5 μm in diameter and 1.2 mm in length. The

RMS value of the velocity component parallel to the axis of the combustion chamber is about 20% less than that of the velocity component normal to the axis of the combustion chamber. Thus the turbulence field is not completely isotropic. The velocity fluctuation indicated that there exists no mean flow at the center of the combustion chamber. Under this condition, the conventional definition of turbulence intensity is meaningless. Therefore, considering symmetry of the combustion chamber, turbulence intensity was defined as the RMS value of the resolved normal and parallel components of velocity, which is given by

$$v' = \left(\frac{2\,{v_r}^2 + {v_z}^2}{3}\right)^{1/2} \tag{1}$$

where

$$v_r = v_L \tag{2}$$

$$v_z = \left({v_H}^2 - {v_L}^2\right)^{1/2} \tag{3}$$

The velocity at two position near the center of the combustion chamber was measured simultaneously by a pair of laser doppler velocimeters to estimate velocity correlation coefficients. The directions of laser beams were adjusted by beam traverse systems. The optical axes of the laser doppler velocimeters crossed each other at 13°. Scattered light from the two positions was detected and processed individually. The velocity at the two position was determined through the correction for the difference of the optical axis directions. An integral length scale L_s, defined as the distance between positions whose correlation coefficient was equal to $1/e$, was obtained from these measurements. Taylor microscale λ and Kolmogorov microscale η were calculated from the integral length scale and the turbulence intensity (5):

$$\frac{\lambda}{L_S} = 15^{1/2}\left(\frac{v' L_S}{\nu}\right)^{-1/2} \tag{4}$$

$$\tag{5}$$

where ν was kinematic viscosity. The value for air at 300 K of 0.1604 cm^2/s was used as ν.

$$\eta = \left(\frac{\nu^3}{\epsilon}\right)^{1/4} \tag{6}$$

where

$$\epsilon = 15\,\nu\,\frac{{v'}^2}{\lambda^2}. \tag{7}$$

The turbulent scales obtained by the above method are shown in Fig. 4.

NUMERICAL MODEL

Distributions of velocity and temperature near the spark gap were calculated by Large Eddy Simulation (LES), in two dimensional cylindrical coordinates. Turbulence models were used in the calculation to treat subgrid scale turbulence. The computational region is shown as Fig. 5. The computational region is 6.4 mm in z direction parallel to the axis of the spark electrode and 3.2 mm in r direction perpendicular to that axis. The spark electrode diameter is 0.2 mm. The spark gap width is 1.0 mm. In the numerical simulation, spark energy was added to the gas in the spark gap as internal energy. The amount of capacitance energy component was controlled by changing the power setting. Spark duration of capacitance component was constant at 1.0 μs. The amount of inductance energy component was controlled by changing the spark duration. The power of the inductance component was constant at 1.0 W. The periodic boundary condition is adopted at the boundaries (1) and (3) in Fig. 5. The free boundary condition is adopted at the boundary (2) in Fig. 5. An isotropic turbulence field having the following energy spectrum (2) was given as initial condition.

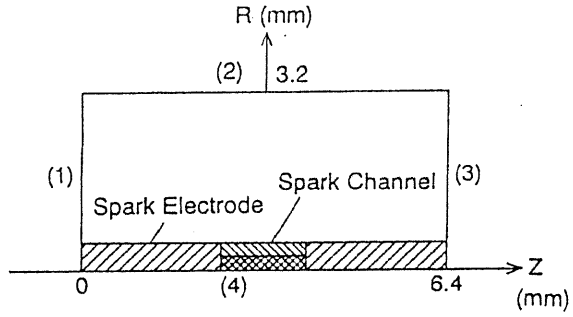

Fig. 5 Computational region

$$E(k) = \frac{8}{\pi}\,{v'}^2\,L_S\,\frac{k^4\,{L_S}^4}{\left(1 + k^2\,{L_S}^2\right)^3} \tag{8}$$

where k is wave number, u' is turbulence intensity, L_S is integral length scale. u' and L_S are 9.87 m/s and 1.23 mm, respectively. In LES, physical quantity f is separated to large scale component $\overline{f}$ and small scale component f' through a space filter, as follows:

$$f = \overline{f} + f' \tag{9}$$

$$\tag{10}$$

where

$$\overline{f(x_1, x_2)} = \iint_{-\infty}^{\infty} f(x_1', x_2') \prod_{i=1}^{2} G_i(x_i, x_i')\,dx_1'\,dy_2' \tag{11}$$

where $G_i(x_i, x_i')$ is a filter function of Gaussian distribution in x_i direction.

$$G_i(x_i, x_i') = \left(\frac{6}{\pi\,\Delta^2}\right)^{1/2} \exp\left(-6\frac{|x_i - x_i'|^2}{\Delta^2}\right) \tag{12}$$

where Δ is filter width. It is equal to the diagonal length of the computational grid. The equations to be resolved were obtained as follows through this filtering and a turbulence model adoption:

$$\frac{\partial \overline{\rho}}{\partial t} + \frac{1}{r}\frac{\partial \overline{\rho v_r}}{\partial r} + \frac{1}{z}\frac{\partial \overline{\rho v_z}}{\partial z} = 0 \tag{13}$$

$$\frac{\partial \overline{\rho v_r}}{\partial t} + \frac{1}{r}\frac{\partial \overline{\rho v_r}\,\overline{v_r}\,r}{\partial r} + \frac{\partial \overline{\rho v_r}\,\overline{v_z}}{\partial z} = -\frac{\partial \overline{p}}{\partial r} + \frac{1}{r}\frac{\partial}{\partial r}(\sigma^m{}_{rr} + \overline{\sigma_{rr}}\,r) + \frac{\partial}{\partial z}(\sigma^m{}_{rz} + \overline{\sigma_{rz}}) - \frac{\overline{\sigma_{\theta\theta}}}{r} \tag{14}$$

$$\frac{\partial \overline{\rho v_z}}{\partial t} + \frac{1}{r}\frac{\partial \overline{\rho v_z}\,\overline{v_r}\,r}{\partial r} + \frac{\partial \overline{\rho v_z}\,\overline{v_z}}{\partial z} = -\frac{\partial \overline{p}}{\partial z} + \frac{1}{r}\frac{\partial}{\partial r}(\sigma^m{}_{rz} + \overline{\sigma_{rz}}\,r) + \frac{\partial}{\partial z}(\sigma^m{}_{zz} + \overline{\sigma_{zz}}) \tag{15}$$

$$\frac{\partial \overline{\rho e}}{\partial t} + \frac{1}{r}\frac{\partial \overline{\rho e}\,\overline{v_r}\,r}{\partial r} + \frac{\partial \overline{\rho e}\,\overline{v_z}}{\partial z} = -\frac{\partial}{\partial r}(\overline{p\,v_r}\,r + J_r\,r - \overline{\sigma_{rr}\,v_r}\,r - \overline{\sigma_{rz}\,v_z}\,r + \overline{q_r}\,r) - \frac{\partial}{\partial z}(\overline{p\,v_z}\,r + J_z - \overline{\sigma_{rz}\,v_z} - \overline{\sigma_{zz}\,v_z} + \overline{q_z}) + \left(\frac{\overline{\partial q}}{\partial t}\right)_C \tag{16}$$

$$\frac{\partial \overline{\rho_i}}{\partial t} + \frac{1}{r}\frac{\partial \overline{\rho_i}\,\overline{v_r}\,r}{\partial r} + \frac{\partial \overline{\rho_i}\,\overline{v_z}}{\partial z} = \frac{1}{r}\frac{\partial}{\partial r}\left(\overline{\rho D \frac{\partial Y_i}{\partial r}}\,r - f_r\,r\right) + \frac{\partial}{\partial z}\left(\overline{\rho D \frac{\partial Y_i}{\partial z}} - f_z r\right) + \left(\frac{\overline{\partial \rho_i}}{\partial t}\right)_C . \tag{17}$$

The model proposed by Smagorinsky et. al. (4) was applied to stress tensor σ^m, and the eddy diffusivity model was applied to heat flux J and mass flux f.

$$\sigma^m{}_{rr} = K\,D_T \tag{18}$$
$$\sigma^m{}_{rz} = K\,D_S \tag{19}$$
$$\sigma^m{}_{zr} = K\,D_S \tag{20}$$
$$\sigma^m{}_{zz} = -K\,D_T \tag{21}$$

$$J_r = -K_E \frac{\partial \overline{\rho e}}{\partial r} \tag{22}$$
$$J_z = -K_E \frac{\partial \overline{\rho e}}{\partial z} \tag{23}$$
$$f_r = -K_C \frac{\partial \overline{\rho_i}}{\partial r} \tag{24}$$
$$f_z = -K_C \frac{\partial \overline{\rho_i}}{\partial z} \tag{25}$$

$$D_T = \frac{\partial v_r}{\partial r} - \frac{\partial v_z}{\partial z} \tag{26}$$

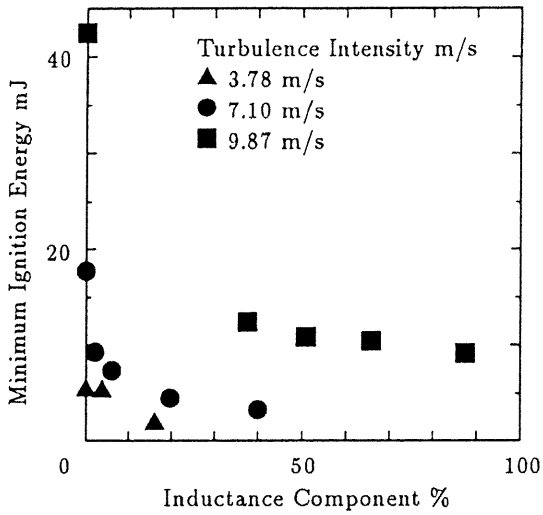

Fig. 6 Minimum ignition energy in experiment

$$D_S = \frac{\partial v_z}{\partial r} + \frac{\partial v_r}{\partial z} \tag{27}$$
$$K = (C\,\Delta)^2\,|D| \tag{28}$$
$$|D| = (D_T{}^2 + D_S{}^2)^{1/2} \tag{29}$$
$$K_E = C_E\,K \tag{30}$$
$$K_C = C_C\,K \tag{31}$$

where C, C_E, and C_C are model constants. C was determined at 0.1 so that the flows containing shock waves caused by spark ignition could be calculated in stable. C_E was decided at 1.4 like Karino (3). C_C was decided at 2.0 like Antonopoulos-Domis (1).

RESULTS AND DISCUSSION

The effect of the inductance component on minimum ignition energy in experiment is shown in Fig. 6. In the case of no inductance component, the minimum ignition energy rapidly increases as turbulence intensity increases. The addition of slight amount of energy of the inductance component improves ignition ability significantly. This effect of inductance component on minimum ignition energy is particularly remarkable in case of high turbulence intensity. This result suggests that composite sparks which includes a high energy inductance component would be beneficial to the ignition of turbulent mixtures. The effect of the inductance component on minimum ignition energy in numerical simulation is shown in Fig. 7. The two results are only in qualitative agreement: in the both results, minimum ignition energy decreases as the inductance component increases. The magnitude difference between predictions and experiments in these results can be explained as below. The numerical simulation in two coordinates can treat only axial eddies so that the eddy viscosity of the turbulence model is smaller than that in the fully three-dimensional case. Consequently, the predicted

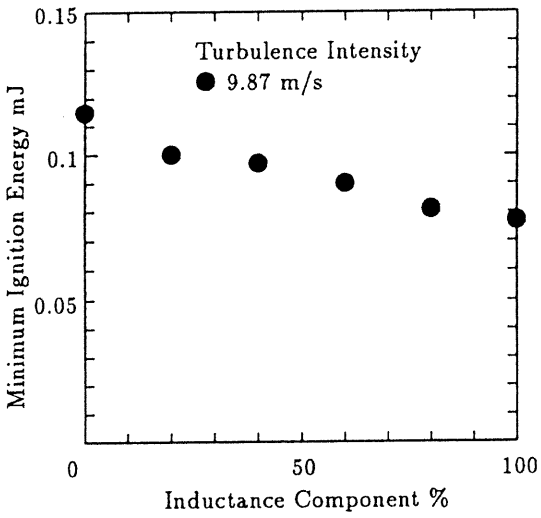

Fig. 7 Minimum ignition energy in numerical simulation

heat transfer by turbulence becomes small.

Distributions of temperature and velocity near the spark gap after the onset of spark discharge obtained by the numerical simulation are shown in Figs. 8 and 9. The solid lines are isothermal lines. The minimum temperature described by one of the isothermal lines is 400 K. The distance of the isothermal lines is equal to 400 K. The allows express magnitude and direction of velocity. The capacitance spark whose energy was 0.11 mJ was used in the numerical simulation of Fig. 8. The composite sparks whose total energy was 0.09 mJ (consisting 20% of capacitance component and 80% of inductance component) was used in the simulation of Fig. 9. In the case of capacitance spark, the flame kernel is brought downstream by the flow near the spark gap as shown in Fig. 8. The flame kernel exists far from the spark gap and is expanded by flow at 160 μs after the onset of spark discharge as shown in Fig. 8. On the contrary, in the case of composite sparks with a high energy inductance component, the flame karnel remains near the spark gap until 160 μs after the onset of spark discharge as shown in Fig. 9.

Turbulence intensity in the spark gap during the ignition process, estimated from the numerical simulation, in the cases of capacitance spark and composite sparks is shown in Fig. 10. In both cases, the turbulence intensity keeps a very high value in the short period just after the start of spark discharge. Then, the turbulence intensity decreases with oscillation. The burst of turbulence intensity is caused by the spark of capacitance component. In the case of capacitance spark, spark discharge has been finished and the flame kernel exists far from the spark gap after the burst of turbulence intensify so that there is no source of turbulence in the spark gap. Consequently, turbulence intensity in the spark gap decreases. Turbulence intensity in the case of high energy inductance component is lower than that in the case of no inductance component

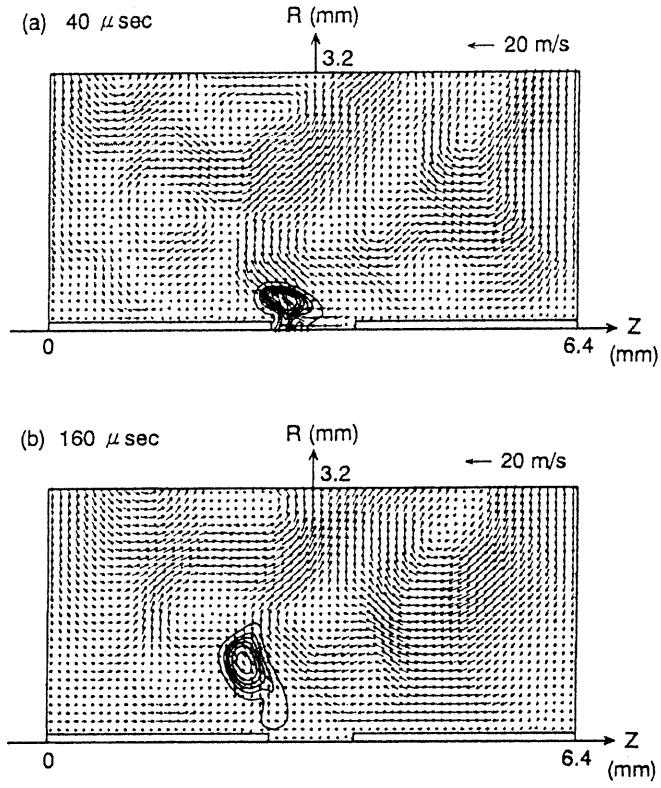

Fig. 8 Distribution of temperature and velocity produced by the capacitance spark

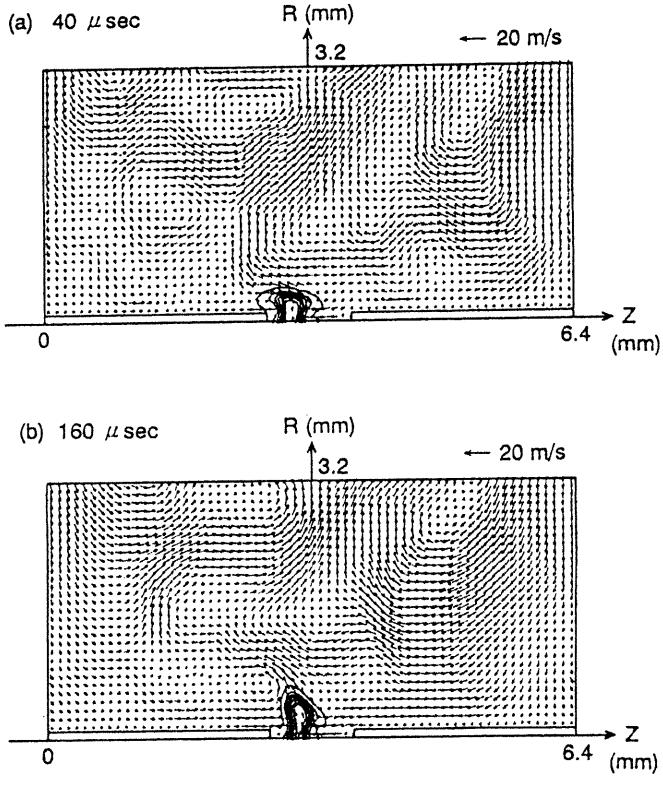

Fig. 9 Distribution of temperature and velocity produced by the composite sparks

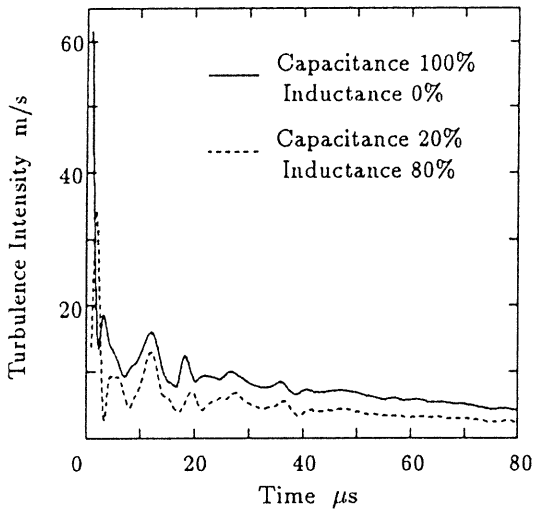

Fig. 10 Turbulence intensity in the spark gap

in spite of the existing of a flame kernel, which is a source of turbulence, in the spark gap. The gas at high temperature and pressure produced by the spark of inductance component prevents entering of turbulence flow into the spark gap. This effect of inductance component has an advantage in spark ignition of turbulent mixtures because a flame kernel is put in the region of low turbulence intensity.

CONCLUSIONS

1. Composite sparks with a high energy inductance component show high ignition ability in turbulent mixtures. This is remarkable in turbulent mixtures of high intensity.
2. Flame kernels develop near the spark gap in case of composite sparks with a low energy capacitance component. On the contrary, flame kernels leave the spark electrodes in early time and develop far from the spark gap in case of composite sparks with a high energy capacitance component.
3. Inductance component has the effect of turbulence suppression in the spark gap during the spark duration. This effect protects flame kernels from expansion by turbulence.

NOMENCLATURE

C = model constant
D_T = strain velocity
D_S = strain velocity
D = diffusion coefficient
E = energy spectrum
e = internal energy
f = mass flux
k = wave number
G = filter function
J = heat flux
K = eddy viscosity
L_S = integral length scale
q = heat release ratio
r = radial coordinate
f = physical quantity
f' = small scale component of physical quantity
$\overline{f}$ = large scale component of physical quantity
t = time
v = velocity
v' = turbulence intensity
Y = mass fraction
z = axial coordinate
Δ = filter width
ϵ = dissipation rate
λ = Taylor microscale
η = Kolmogorov microscale
ν = kinematic viscosity
ρ = density
σ = stress tensor
σ^m = stress tensor transformed by turbulence model

Subscripts
C = chemical reaction
E = internal energy
H = measured by hot wire anemometer
i = chemical species
L = measured by laser doppler velocimeter
r = radial component
z = axial component
θ = circumference component

REFERENCES

1. Antonopoulos-Domis, M., "Large-Eddy Simulation of A Passive Scalar in Isotropic Turbulence," Journal of Fluid Mechanics Vol. 104, pp. 55-79, 1981.
2. Hinze, J. O., Turbulence, McGraw-Hill, New York, pp. 211, 1987.
3. Kano, M., Kobayashi, T. and Ishihara, T., "Prediction of Turbulent Flow in Two-Dimensional Channel with Turbulence Promoters," Transactions of the Japan Society of Mechanical Engineers (in Japanese) Vol. 50(B), No. 449, pp. 257-264, 1987.
4. Smagorinsky, J., Manabe, S. and Holloway, J. L. Jr., "Numerical Results from A Nine-level General Circulation Model of The Atmosphere," Monthly Weather Review Vol. 93, No. 12, pp. 727-768, 1965.
5. Tennekes, H. and Lumley, J. L., A First Course in Turbulence, The MIT Press, pp. 67, 1972.